Saturation-Based Adaptive Tracking Control of Underwater Vehicles: From Theoretical Design to Real-Time Experiments

Auwal Tijjani Shehu, Ahmed Chemori, Vincent Creuze

Saturation-Based Adaptive Tracking Control of Underwater Vehicles: From Theoretical Design to Real-Time Experiments

Auwal Shehu Tijjani, *Member, IEEE*, Ahmed Chemori, *Senior Member, IEEE*, and Vincent Creuze

Abstract—Tracking control of an autonomous tethered underwater vehicle (ATUV) for a successful marine operation is a challenging task due to the complex and nonlinear dynamics of the vehicle characterized by parametric uncertainties. Besides these issues, the vehicle mainly operates in an uncertain and unpredictable environment. To deal with the ATUV control tracking problem, this paper proposes a new tracking control approach that will be named saturation-based adaptive computed torque+ (SACT+). The proposed SACT+ is designed using a variable saturation function, a computed torque structure, a saturation-based dynamic feedback, and an adaptive mechanism. Then, several arguments, based on the well-known Lyapunov techniques, are proposed to prove the stability behavior of the final closed-loop dynamics. This ensures the convergence (theoretically) of the vehicle tracking error to the origin, leading to stable and safe operations. However, this tracking error (experimentally) only stays around the origin due to many factors, such as the measurement noise from the vehicle's sensors, the inherent uncertainties of the vehicle combined with external disturbances from the marine environment, etc. Different tests are conducted in real-time using our underwater vehicle *Leonard* prototype to validate the proposed SACT+. The obtained experimental results show the effectiveness and robustness of the proposed SACT+ approach in real-life cases. Finally, the performance and energy consumption indices, as well as comparative experimental studies with two well-established controllers (from the literature), confirm the relevance of the proposed approach for controlling small-sized and/or low-cost underwater vehicles.

Index Terms—Underwater vehicles, adaptive control, computed torque, trajectory tracking, saturation function, stability analysis, extensive real-time tests.

I. INTRODUCTION

UNDERWATER environments, occupying approximately 71% of the Earth's surface, represent an invaluable amount of natural resources, which are essential for the wildlife, the humans, and the industry [1]. Exploring and exploiting these environments in a sustainable manner should provide large benefits for a better quality of life for humanity [2]. However, most of the seas remain poorly known because of the difficult access to this harsh environment. In order to improve the ability to explore and exploit the underwater environment, intelligent tools are required, in addition to the conventional ways used in the past decades, such as divers or manned submarines.

For these reasons, many researchers have proposed safe and fast techniques for exploring these environments more efficiently, more accurately, and at cheaper costs, for instance, using unmanned underwater vehicles (UUVs) or robots [3], [4]. As a result, these vehicles become recently a hot research topic since they can remotely or autonomously extend the observation and activities of humans into the underwater environments [5]. Hence, the robots are now used in an increasing number of marine applications. Moreover, the global market of UUVs is expected to reach approximately up to 1 billion USD by the near future [6]. One of the most challenging aspects related to UUVs lies in designing an autonomous robust control scheme for the vehicle [7], [8]. Even though new control schemes for autonomous UUVs are always evolving, many of them are not validated in real-time on actual vehicles due to their complexities [9]. Hence, the conventional PD and PID control schemes gain more place and a much higher rating in real-time control of UUVs compared to the advanced/robust control techniques [10]. Unfortunately, in real-time marine applications, the performances of these classical control schemes are often degraded [11]. Furthermore, the classical control schemes may generate control signals beyond the UUV's actuators saturation limits when counteracting the negative effect of uncertainties/external disturbances [12]. To deal with these drawbacks, several advanced control methods have been proposed in the literature.

In order to study the performance of various tracking control schemes for UUVs, an experiment-based survey has been conducted in [11]. A nonlinear observer-based PID has been proposed to control the position and orientation of a fully actuated remotely operated vehicle (ROV) equipped with a gripper in [13]. Even though the obtained results demonstrate the effectiveness of the proposed controller in simulation, the stability analysis of the closed-loop system has not been conducted. Indeed, only one simulation scenario has been tested. Furthermore, in [14], a PI-PID controller has been proposed to control the roll, pitch, and depth of an underwater towfish for monitoring water pollution. Although the proposed PI-PID has been implemented and tested on the towfish in the Strait of Sicily, the stability of the final closed-loop dynamics has not been proven (theoretically). To reduce the computational cost and the training time of a neural-network-based

Auwal Shehu Tijjani (e-mail: auwal-tijjani.shehu@lirmm.fr), Ahmed Chemori (e-mail: ahmed.chemori@lirmm.fr), and Vincent Creuze (vincent.creuze@lirmm.fr) are affiliated with LIRMM (Laboratory of Computer Science, Robotics, and Microelectronics), University of Montpellier, CNRS, Montpellier, France.

PID controller, a single-layer learning-based PID controller has been proposed in [15]. Although the proposed controller has been experimentally tested on *Sailfish*, its stability for marine applications has not been proven analytically. Also, this controller requires some knowledge about the system dynamics. Nonetheless, obtaining an exact dynamics remains a difficult task within control system research communities [16].

Considering the highly uncertain nature and stochastic external disturbances in marine environments, many researchers proposed adaptive control techniques for solving UUVs tracking problems. Since adaptive control is a wide field of research, in the sequel, we focus on reviewing the main recently proposed adaptive control schemes in literature in the context of UUVs. An adaptive nonlinear dynamic controller has been proposed for a desired reference path tracking of UUVs in [17]. To improve the computational speed and preserve the robustness of this controller, the proposed adaptation law estimates the matrices of the vehicle's dynamics instead of estimating its dynamic parameters. Recently, a deep reinforcement learning-based (RL) adaptive control for UUVs has been proposed in [18]. The proposed approach is an attempt to reduce the computational cost and the energy consumption associated with classical RL through a modified RL architecture known as actor-critic goal-oriented deep RL. Furthermore, the depth tracking problem of UUVs has been addressed using RL based on the batch-gradient update technique in [16]. This approach may be considered as a step forward to reaffirm the place of model-free RL control in dealing with UUVs tracking problems, despite the vehicle's limited hardware resources [19]. However, real-time experiments are needed to validate the scheme in [16]. In [20], target tracking problems for UUVs have been addressed using an adaptive fuzzy controller. An adaptive fault-tolerant control has been proposed in [21] to demonstrate the high efficiency of an adaptive-based scheme in the case of vehicle actuators' saturation and failure during a marine mission. Note that most of these schemes aim to compensate for the effects of actuators' saturation and reject external disturbances [22]. However, the complex nature of marine applications triggers the aggressive behavior of the majority of these schemes, generating control signals beyond mechanical actuators' limits; this issue often leads to mission shutdown.

In the literature, we can critically notice that the majority of the proposed control schemes for UUVs require a velocity measuring sensor, such as a Doppler Velocity Logger (DVL), which is quite expensive [11]. To address this issue, a nonlinear integral adaptive-based control has been proposed in [23]. Even though the proposed control in [23] has been validated in simulation as well as real-time experiments, further scenarios need to be tested to confirm its effectiveness. On the other hand, the proposed control approach has the advantage of being a simple technique; however, this control approach may require more improvement in a marine application, where high-precision tracking is a priority.

While extending the control law proposed in [24] and reminded at the beginning of Section III to the case of real-time marine missions of UUVs, we faced several challenges. This work proposes a new control scheme to address these issues and to deal with the control tracking problem. The proposed control scheme takes into account the main constraints, including (i) the limitation of the system's hardware resources, (ii) the simplicity and the affordable cost of the implementation process in real-time, and (iii) the highly uncertain nature of the marine environment. The contributions of this research work are summarized as follows:

1) We propose a new control approach denoted Saturation-based adaptive computed torque+ (SACT+), which exploits the advantages of the computed torque (CT) structure, a saturation-based dynamic mechanism, a variable saturation function, and an adaptation law to resolve the tracking control problem of UUVs in marine applications. Even though a literature survey revealed a lot of works on classical CT applied to other robotic systems, to the best knowledge of the authors, only a few previous works exist on applications of this control scheme to UUVs. Indeed, the proposed SACT+ can be considered as a new approach. Besides being a computationally light scheme, the proposed SACT+ control law takes into account the saturation of the robot actuators. Also, the proposed controller dynamically compensates the UUV's dynamics through the saturation-based dynamic filtering mechanism, which contrariwise the exact dynamic compensation in the case of [24].
Compared to the controller recently proposed in [25], the proposed SACT+ control scheme exploits the inertia of the vehicle's dynamics to improve tracking error and reduce energy consumption. Moreover, in the architecture of the proposed SACT+ scheme, the highly uncertain terms (e.g., hydrodynamics) are dynamically compensated; this contradicts the case of [25], where constant feedforward terms have been used to compensate for the vehicle's dynamics. On the other hand, the controllers developed in [26] and [27] estimate all the dynamics of the vehicle. However, these controllers generate high control inputs. Additionally, the control scheme proposed in [28] relies explicitly on the measurement of the velocity signal. Nevertheless, the measurement of velocity signals is not available in many real systems [29], including our vehicle, due to the expensive cost.
2) Lyapunov arguments are employed to prove the stability of the resulting closed-loop dynamics, which guarantees a stable operation during marine missions.
3) Scenarios-based real-time experiments are conducted to prove the efficiency and robustness, as well as the external disturbance rejection of the proposed SACT+ approach.
4) We further investigate the performance of the proposed SACT+ through comparative experimental studies with the classical CT in [30], [31], and intelligent fuzzy control (IFC) proposed recently in [22]. Finally, a tuning algorithm of the proposed SACT+ scheme parameters is provided in this paper.

The subsequent sections of this paper are organized as follows. Section II describes the vehicle used to validate the proposed
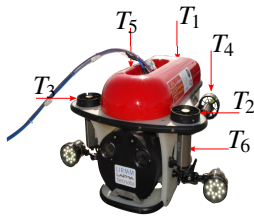
Fig. 1. View of *Leonard* underwater vehicle with its six independent thrusters, which generate forces to actuate the vehicle along its six degrees of freedom.

SACT+ scheme and its related modeling process. The proposed SACT+ control scheme design and its stability analysis are introduced in Sections III and IV, respectively. Then experimental results are presented and discussed in Section V. Section VI finalizes this paper with some concluding remarks and possible future extensions of the proposed SACT+ control approach.

II. System Description and Modeling

In this section, we describe in detail the main features as well as the mathematical modeling of the vehicle used for validating the proposed control scheme.

A. Vehicle Description

The proposed SACT+ scheme (described in Section III) is implemented in real-time experiments on an underwater vehicle prototype named *Leonard*, illustrated in Fig. 1. This vehicle was designed and entirely made at *LIRMM*, a robotics laboratory of the University of Montpellier. Some of the main features of this vehicle, worth to be mentioned to facilitate its modeling process, are summarized as follows:

1) *Leonard* is a holonomic underwater vehicle equipped with 6 thrusters placed as illustrated in Fig. 1.
2) Due to the low position of its center of gravity, the *Leonard* ATUV is designed to be naturally stable in roll ϕ and pitch θ.
3) The vehicle can be operated either (i) as an autonomous vehicle or (ii) via shared control (a human pilot operating remotely). The summary of the vehicle's components and parameters specifications are given in TABLE I.

B. Vehicle Modeling Process

Many research communities studied the mathematical modeling of underwater vehicles [28]. In this paper, we take into account the parametric uncertainties in the vehicle dynamics. The kinematics and dynamics of the vehicle considered in this work, are presented in the following.

1) Leonard's kinematics: Let us define R_i and R_v as the inertial and vehicle reference frames (Fig. 2), respectively. We can express the position and orientation of the vehicle in the frame R_i as $\eta = [\eta_1^T \ \eta_2^T]^T$, the velocity in the frame R_v as $v = [v_1^T \ v_2^T]^T$; where $\eta_1 = [x \ y \ z]^T \in \mathbb{R}^{3 \times 1}$ is the position coordinates vector, $\eta_2 = [\phi \ \theta \ \psi]^T \in \mathbb{R}^{3 \times 1}$ denotes the Euler angles orientation coordinates vector, $v_1 = [u \ v \ w]^T \in \mathbb{R}^{3 \times 1}$ represents the linear velocity vector, $v_2 = [p \ q \ r]^T \in \mathbb{R}^{3 \times 1}$

TABLE I
SUMMARY OF *LEONARD* ATUV'S COMPONENTS AND PARAMETERS

Components and Parameters	Descriptions and Specifications
Attitude Sensing Module	Sparkfun MPU (9250), MEMS 9-axes gyrometer, accelerometer, and magnetometer.
Depth Sensing Module	MS5803-14BA pressure sensing module.
Dimensions	750mm (L) × 550mm (W) × 450mm (H).
Floatability	≈ 9N.
Light	LED with rating of 50W.
Mass	≈ 28kg.
Depth Range	[0 - 100]m, proportional to the limit of the depth sensor.
Sampling Period	≈ 50ms.
Surface Computer	Dell Latitude (E6230s) i7-3520M@2.9GHz, 32 GB of RAM, 64-bit Windows 11 OS, Microsoft Visual IDE (C++) 2022.
Power Rating	24V with rating of 600W.
Vehicle Tether	≈ 50m.
Thrusters/Propellers	6-Seabotix (BTD150 equipped with Syren 10 drivers) continuous thrust of 2.2kgf each.

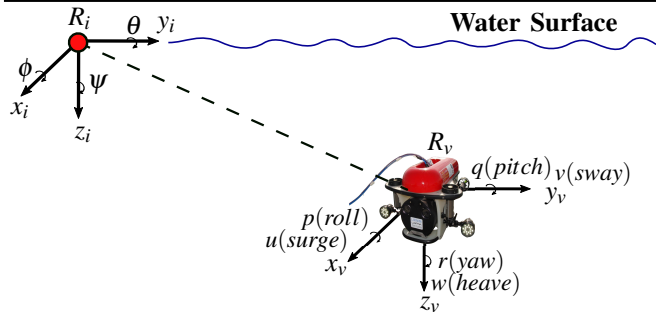

Fig. 2. *Leonard's* assigned reference frames (inertial frame R_i and body fixed frame R_v) to facilitate its mathematical modeling and control.

represents the angular velocity vector. Then, the vehicle's kinematics can be expressed as:

$$\dot{\eta} = J(\eta)v \quad (1)$$

where $J(\eta) \in \mathbb{R}^{6 \times 6}$ is the so-called transformation matrix.
Remark 1: *The vehicle kinematics (1) is well defined and invertible under a constraint, as it is only defined for a marine mission when the maximum vehicle's pitch angle satisfies $|\theta|_{max} < \frac{\pi}{2}$, to avoid a potential singularity in the matrix $J(\eta)$ caused by Euler angles representation. In some applications where $\theta \to \pm\frac{\pi}{2}$, the quaternions are preferred to describe the state vector of the vehicle [32].*
Based on *remark 1*, in this work, we consider the case where the desired pitch θ_d is sufficiently far away from the neighborhood of $\theta = \pm\frac{\pi}{2}$; hence, (1) is well defined.

2) Leonard's dynamics: Inspired by [28] and the formulations proposed in [8], the six-degree-of-freedom *Leonard's* dynamics expressed in the frame R_v (illustrated in Fig. 2) using the SNAME notation can be written as follows:

$$M\dot{v} + C(v)v + D(v)v + g(\eta) = \tau + \chi(t) \quad (2)$$

where $M \in \mathbb{R}^{6 \times 6}$ is the system inertia matrix including the effect of added mass, $C(v) \in \mathbb{R}^{6 \times 6}$ is the hydrodynamic Coriolis/centripetal matrix, $D(v) \in \mathbb{R}^{6 \times 6}$ represents the hydrodynamic lift and damping matrix where the quadratic and

linear effects are included, $g(\eta) \in \mathbb{R}^{6 \times 1}$ is the vector of gravity/buoyancy induced forces and moments, $\tau \in \mathbb{R}^{6 \times 1}$ is the vector of inputs containing control signals (generated by the thrusters of the vehicle) and $\chi(t) \in \mathbb{R}^{6 \times 1}$ denotes the external disturbances (time-varying, e.g., water currents) vector, while v and η are as defined in (1).

The matrices M and $C(v)$ in (2) are given by:

$$\begin{cases} M = M_{RB} + M_A \\ C(v) = C_{RB}(v) + C_A(v) \end{cases} \tag{3}$$

where M_{RB} is the rigid-body inertia and M_A is the inertia of the added mass. $C_{RB}(v)$ and $C_A(v)$ denote respectively the rigid-body and hydrodynamics of Coriolis and centripetal matrices. The damping matrix $D(v)$ is expressed in R_v as (see [25] and [5] for further details) follows:

$$D(v) = D(v)_L + D(v)_Q \tag{4}$$

where $D(v)_Q \in \mathbb{R}^{6 \times 6}$ is the quadratic damping effect, $D(v)_L \in \mathbb{R}^{6 \times 6}$ is the linear damping effect, and $D(v)$ has been defined previously in (1). It is worth noting that $D(v)$ is strictly positive (i.e., $D(v) > 0$, $\forall v \in \mathbb{R}^{6 \times 1}$), and the matrix $D(v)_L$ of our vehicle have been experimentally identified in [5].

The vector $g(\eta)$ can be expressed as follows:

$$g(\eta) = \begin{bmatrix} F_{g(\eta)} \\ M_{g(\eta)} \end{bmatrix} \tag{5}$$

where $F_{g(\eta)} \in \mathbb{R}^{3 \times 1}$ and $M_{g(\eta)} \in \mathbb{R}^{3 \times 1}$ are the vectors of restoring forces and moments, respectively (see [5] for more details).

Finally, the vector τ is expressed in terms of the control input forces and moments generated by the thrusters and is given by:

$$\tau = \underline{B} u \tag{6}$$

where $\underline{B} \in \mathbb{R}^{6 \times 6}$ is the thrusters configuration matrix of the vehicle and $u \in \mathbb{R}^{6 \times 1}$ is a vector of forces, with elements $T_1, T_2, .., T_6$, generated for the navigation of the vehicle by its thrusters (as illustrated in Fig. 1).

Remark 2: *It is worth to note that the matrices of the vehicle dynamics M and $C(v)$ (in (3)) are partially known, $D(v)$ (in (4)) is highly unknown, while the vector $g(\eta)$ (in (5)) is approximately known and the control inputs vector τ (in (6)) is well known by design. The uncertainties in these parameters are mainly due to the hydrodynamics effects and the modeling.* Even though the dynamics of underwater vehicles is decomposed into nominal and uncertain parts in the literature, not all the parametric uncertainties/perturbations are considered. Hence, we propose to improve the representation in (2) based on *remark 2*, by including all the necessary uncertainties/perturbations as follows:

$$M^\star \dot{v} + C^\star(v) v + D^\star(v) v + g^\star(\eta) = \tau^\star \\ \underbrace{- [\Delta M \dot{v} + \Delta C(v) v + \Delta D(v) v + \Delta g(\eta) + \underline{\chi}(t)]}_{\chi^\star(t)} \tag{7}$$

where the terms from (2) can be expressed as $\varphi(\cdot) = \varphi^\star(\cdot) + \Delta\varphi(\cdot)$ in (7), with $\varphi^\star(\cdot)$ the known part of the ATUV's model parameters and $\Delta\varphi(\cdot)$ the completely/partially

unknown part of each dynamics parameter. Thus, the certain version of $\varphi(\cdot)$ is $\varphi^\star(\cdot) \in \{M^\star, C^\star(v), D^\star(v), g^\star(\eta)\}$, $\tau^\star = \tau$, $\underline{\chi}(t) = -\chi(t)$ is assumed as a model of water currents proposed in [28] while $\chi^\star(t)$ is the lumped disturbance vector of parametric uncertainties combined with time-varying water currents.

To facilitate the proposed control scheme design and its stability analysis in the subsequent sections, the vehicle dynamics (7) is transformed to the frame R_i using the following:

$$\begin{cases} \ddot{\eta} = J(\eta) \dot{v} + \dot{J}(\eta) v, \ M_\eta^\star(\eta) = J^{-T}(\eta) M^\star J^{-1}(\eta), \\ C_\eta^\star(v, \eta) = J^{-T}(\eta) [C^\star(v) - M^\star J^{-1}(\eta) \dot{J}(\eta)] J^{-1}(\eta), \\ D_\eta^\star(v, \eta) = J^{-T}(\eta) D^\star(v) J^{-1}(\eta), g_\eta^\star(\eta) = J^{-T}(\eta) g^\star(\eta), \\ \tau_\eta^\star(\eta) = J^{-T}(\eta) \tau^\star \ \text{and} \ \chi_\eta^\star(t) = J^{-T}(\eta) \chi^\star(t). \end{cases}$$

Thus, the improved vehicle's dynamics is expressed as follows:

$$M_\eta^\star(\eta) \ddot{\eta} + C_\eta^\star(v, \eta) \dot{\eta} + D_\eta^\star(v, \eta) \dot{\eta} + g_\eta^\star(\eta) = \tau_\eta^\star(\eta) - \chi_\eta^\star(t) \tag{8}$$

where, all the terms of the dynamics (8) have been defined in (2), prior to the transformation into R_i.

III. PROPOSED CONTROL SCHEME

In this section, the design of the proposed SACT+ control scheme for trajectory tracking of underwater vehicles is introduced. This control approach is inspired from the classical CT structure [30], [31], and the NLCT proposed in [24]. The NLCT approach in [24] does not take into account the saturation of the robot actuators. As a result, high control feedback gains may lead to actuator damage. Besides not being implemented on systems such as underwater vehicles where the effects of hydrodynamics are high, the NLCT suppresses many interesting nonlinear closed-loop dynamics behaviors. Also, the impact of unpredictable external disturbances, such as a sudden collision with the environment, is not considered.

For all these reasons, we propose to counteract the drawbacks of the NLCT through the redesign of the whole control structure to suit other systems like UUVs, as follows. First, we propose to replace the PD control term in the CT structure with a modified PD based on a saturated nonlinear architecture to deal with the problem of actuator saturation and ensure that the tracking error converges near the origin. Then, an adaptation law is integrated into the proposed SACT+ scheme to overcome the effects of restoring forces and moments uncertainties, as well as external disturbances. Also, a saturation-based dynamic mechanism is added to the controller to neutralize the Coriolis effect and hydrodynamics in real-time marine applications. It is worth noting that this mechanism can be easily extended to deal with the negative influence of friction in other dynamical systems. Moreover, we extend the proposed SACT+ scheme to the high order dynamics, for instance, coupled multiple-input multiple-output nonlinear dynamics. Finally, the proposed SACT+ control scheme is implemented on *Leonard* ATUV. The design of the proposed SACT+ approach is given in the sequel.

First, let us consider a predefined desired trajectory $\eta_d(t)$ as,

$$\eta_d(t) = [x_d(t), y_d(t), z_d(t), \phi_d(t), \theta_d(t), \psi_d(t)]^T \tag{9}$$

This article has been accepted for publication in IEEE Transactions on Systems, Man, and Cybernetics: Systems. This is the author's version which has not been fully edited and content may change prior to final publication. Citation information: DOI 10.1109/TSMC.2024.3412797

5

Assumption 1: $\eta_d(t)$ *in (9), and its successive time derivatives, are assumed to be continuous and bounded through a careful design [5].*

Similarly, the actual vehicle's trajectory $\eta(t)$ is defined as:

$$\eta(t) = [x(t), y(t), z(t), \phi(t), \theta(t), \psi(t)]^T \tag{10}$$

Then, the vehicle's tracking error $e(t)$ can be expressed as:

$$e(t) = \eta_d(t) - \eta(t) \tag{11}$$

where $e(t) = [e_1(t), e_2(t), ..., e_6(t)]^T$, with $\eta_d(t)$ and $\eta(t)$ previously defined in (9) and (10), respectively.

Taking the time derivative of (11) leads to:

$$\dot{e}(t) = \dot{\eta}_d(t) - \dot{\eta}(t) \tag{12}$$

where $\dot{\eta}_d(t)$, $\dot{\eta}(t)$, and $\dot{e}(t) = [\dot{e}_1(t), \dot{e}_2(t), ..., \dot{e}_6(t)]^T$ are the time derivatives of $\eta_d(t)$, $\eta(t)$, and $e(t)$, respectively.

At this stage, let us introduce the design of the saturation-based architecture $\bar{\tau}$ to be included in the proposed SACT+ structure:

$$\bar{\tau} = \sigma_{\bar{s}p}[K_p e(t)] + \sigma_{\bar{s}d}[K_d \dot{e}(t)] \tag{13}$$

where K_p and K_d are matrices containing feedback gains, and where $\sigma_{\bar{s}p}$ and $\sigma_{\bar{s}d}$ are saturation functions. Note that these functions are also exploited in the design of the dynamic filtering mechanism to guarantee that the filter does not grow indefinitely large to contribute to a high value of $\tau^\star$ (beyond actuators' limits). The saturation function is defined as follows:

$$\sigma_{\bar{s}}(f) = \begin{cases} \bar{s} & \text{if} \quad f > \bar{s} \\ f & \text{if} \quad |f| \leq \bar{s} \\ -\bar{s} & \text{if} \quad f < -\bar{s} \end{cases} \tag{14}$$

with $\bar{s}$ defines the limits (upper and lower) of the function, while f represents the function in its linear region.

Equation (13) can be detailed as:

$$\begin{aligned} \sigma_{\bar{s}p}[K_p e(t)] &= diag\{u_{p1}, u_{p2}, ..., u_{p6}\} \\ \sigma_{\bar{s}d}[K_d \dot{e}(t)] &= diag\{u_{d1}, u_{d2}, ..., u_{d6}\} \end{aligned} \tag{15}$$

And thus, considering (14), we have:

$$u_{pi} = \begin{cases} \bar{s}_{pi} & \text{if} \quad k_{pi}f_{pi} > \bar{s}_{pi} \\ k_{pi}f_{pi} & \text{if} \quad |k_{pi}f_{pi}| \leq \bar{s}_{pi} \quad i = \overline{1,6} \\ -\bar{s}_{pi} & \text{if} \quad k_{pi}f_{pi} < -\bar{s}_{pi} \end{cases} \tag{16}$$

$$u_{di} = \begin{cases} \bar{s}_{di} & \text{if} \quad k_{di}f_{di} > \bar{s}_{di} \\ k_{di}f_{di} & \text{if} \quad |k_{di}f_{di}| \leq \bar{s}_{di} \quad i = \overline{1,6} \\ -\bar{s}_{di} & \text{if} \quad k_{di}f_{di} < -\bar{s}_{di} \end{cases} \tag{17}$$

Hence, for each $i \in \{1, ..., 6\}$, we have:

$$\bar{\tau}_i = u_{pi} + u_{di} = k_{pi}(\cdot)e_i(t) + k_{di}(\cdot)\dot{e}_i(t) \tag{18}$$

where the nonlinear gains are defined as:

$$k_{pi}(\cdot) = \begin{cases} \bar{s}_{pi}|e_i(t)|^{(\delta_{pi}-1)} & \text{if} \quad |e_i(t)| > d_{pi} \\ \\ \bar{s}_{pi}d_{pi}^{(\delta_{pi}-1)} & \text{if} \quad |e_i(t)| \leq d_{pi} \end{cases} i = \overline{1,6} \quad (19)$$

$$k_{di}(\cdot) = \begin{cases} \bar{s}_{di}|\dot{e}_i(t)|^{(\delta_{di}-1)} & \text{if} \quad |\dot{e}_i(t)| > d_{di} \\ \\ \bar{s}_{di}d_{di}^{(\delta_{di}-1)} & \text{if} \quad |\dot{e}_i(t)| \leq d_{di} \end{cases} i = \overline{1,6} \quad (20)$$

where $d_{pi} = \frac{\bar{s}_{pi}}{k_{pi}}$ and $d_{di} = \frac{\bar{s}_{di}}{k_{di}}$ are obtained from (16) and (17) respectively, while $\delta_{pi} \in [0,1]$, $\delta_{di} \in [0,1]$ are design parameters selected to determine the shape of the saturation function.

Therefore, we can rewrite (13) as follows:

$$\bar{\tau} = K_p(\cdot)e(t) + K_d(\cdot)\dot{e}(t) \tag{21}$$

where $K_p(\cdot) = diag\{k_{p1}(\cdot), k_{p2}(\cdot), ..., k_{p6}(\cdot)\} > 0$ and $K_d(\cdot) = diag\{k_{d1}(\cdot), k_{d2}(\cdot), ..., k_{d6}(\cdot)\} > 0$ are nonlinear gain matrices. Next, the proposed SACT+ scheme for the six-degree-of-freedom underwater vehicle dynamics in (8) is designed as follows:

$$\begin{aligned} \tau^\star = J^T(\eta)\Big[&(C_\eta^\star(v,\eta) + D_\eta^\star(v,\eta))(\dot{\eta}_d - \alpha_1\Lambda) \\ &+ M_\eta^\star(\eta)(\ddot{\eta}_d + \bar{\tau}) + \Phi_\vartheta\hat{\vartheta}^T \Big] \end{aligned} \tag{22}$$

where $\tau^\star = [\tau_x^\star, \ \tau_y^\star, \ \tau_z^\star, \ \tau_\phi^\star, \ \tau_\theta^\star, \ \tau_\psi^\star]^T$ is the vector of control inputs, Λ is the saturation-based dynamic mechanism vector, $\hat{\vartheta}$ is a vector of the unknown dynamic parameters to be estimated, Φ_ϑ is a regressor matrix and $\alpha_1 = diag\{\alpha_{11}, \alpha_{12}, \cdots, \alpha_{16}\} > 0$ is a strictly positive definite design matrix. The linearity property of the UUV dynamics w.r.t its parameters is exploited to design Φ_ϑ and $\hat{\vartheta}$ for the terms $g_\eta^\star(\eta)$ and $\chi_\eta^\star(t)$ affecting the steady-state of the vehicle. These terms are formulated as, $\Phi_\vartheta = [\Phi_{g_\eta^\star(\eta)}, \Phi_{\chi_\eta^\star(t)}]$ and $\hat{\vartheta}^T = [\hat{\vartheta}_{g_\eta^\star(\eta)}, \hat{\vartheta}_{\chi_\eta^\star(t)}]^T$. Where $\Phi_{g_\eta^\star(\eta)}$ and $\Phi_{\chi_\eta^\star(t)} = J(\eta)$ are the regressor matrices of $g_\eta^\star(\eta)$ and $\chi_\eta^\star(t)$, respectively. $\hat{\vartheta}_{g_\eta^\star(\eta)} = [(B-W), r_{Gz}B]$ (see Appendix B of [5] for the detailed expressions of buoyancy B and weight W while r_{Gz} defines the z-component of the vehicle's center of gravity) and $\hat{\vartheta}_{\chi_\eta^\star(t)} = [\chi_x^\star, \chi_y^\star, \chi_z^\star, \chi_\phi^\star, \chi_\theta^\star, \chi_\psi^\star]$ are the estimates of the unknown parameters of $g_\eta^\star(\eta)$ and $\chi_\eta^\star(t)$ (*lumped disturbance vector of parametric uncertainties combined with time-varying water currents, for further details of water currents model see [28]*), respectively.

The saturation-based dynamic mechanism vector Λ is obtained through a filtering of $e(t)$ and $\dot{e}(t)$ as follows:

$$\dot{\Lambda} = -[\Lambda(0) + K_p(\cdot)e(t) + K_d(\cdot)\dot{e}(t)] \tag{23}$$

While the $\hat{\vartheta}$ in (22) is updated by an adaptation law designed as follows:

$$\dot{\hat{\vartheta}} = \Gamma_\vartheta^{-1}\Phi_\vartheta e_a \tag{24}$$

where $e_a = \dot{e}(t) + \alpha_2 e(t)$, $\alpha_2 = diag\{\alpha_{21}, \alpha_{22}, \cdots, \alpha_{26}\} > 0$, is a positive design matrix and $\Gamma_\vartheta^{-1} = diag\{\gamma_1, \gamma_2, ..., \gamma_6\} > 0$ is the matrix of adaptation gain.

Remark 3: *The vehicle dynamics matrix $D(v)$ (in (4)) is highly unknown and comprises many dynamic elements ([28]). Hence, estimating this matrix online may lead to a too high computational cost in small vehicles with limited hardware resources. To reduce the computational burden and counteract the effect of $D(v)$, a saturation-based dynamic feedback mechanism is proposed in this work.*

IV. CLOSED-LOOP STABILITY ANALYSIS

In this section, we address the stability analysis of the resulting closed-loop system dynamics.

Theorem 1: *The trajectory $\eta(t)$ of an underwater vehicle whose dynamics is defined by (8), under the proposed SACT+ controller designed in (22), (23), and (24), is bounded and converges uniformly to the desired trajectory $\eta_d(t)$ in spite of time-varying external disturbances and parametric uncertainties, provided that the following conditions are fulfilled:*
(i) the feedback gains matrices, $K_p(\cdot) > 0$ and $K_d(\cdot) > 0$ are selected sufficiently enough with respect to the initial tracking error. Note: $K_{p\min} \leq K_p(\cdot) \leq K_{p\max}$ and $K_{d\min} \leq K_d(\cdot) \leq K_{d\max}$, where $K_{p\min}$, $K_{d\min}$, $K_{p\max}$, and $K_{d\max}$ are the minimum and maximum of $K_p(\cdot)$ and $K_d(\cdot)$, respectively. Therefore, $K^\star_{(\cdot)\min} = min\{k_{(\cdot)1\min}, k_{(\cdot)2\min}, ..., k_{(\cdot)6\min}\}$ and $K^\star_{(\cdot)\max} = max\{k_{(\cdot)1\max}, k_{(\cdot)2\max}, ..., k_{(\cdot)6\max}\}$, where $(\cdot) \in \{p, d\}$.
(ii) the following control parameters are designed as, $\alpha_{1i} < \frac{K^\star_{p\min} + K^\star_{d\min}}{D^\star_{\eta i}(v,\eta)[1+\alpha_{2i}]}$ and $\alpha_{2i} < K^\star_{d\min}$ with $i = \overline{1,6}$, and the matrix $\Gamma^{-1}_\vartheta > 0$. As long as these conditions are satisfied, then $e(t)$ will be bounded and converges uniformly around the origin and stay there for all the time.

Proof: To facilitate this analysis, it is necessary to obtain the closed-loop dynamics resulting from the application of the proposed SACT+ control law to the vehicle. To this end, the closed-loop dynamics is obtained as follows. First, we begin by taking the first time-derivative of e_a and multiplying both sides of the obtained equation by $M^\star_\eta(\eta)$ as follows.

$$M^\star_\eta(\eta)\dot{e}_a = M^\star_\eta(\eta)[\ddot{e} + \alpha_2 \dot{e}] \tag{25}$$

Substituting the vehicle dynamics in (8) into (25), leading to:

$$M^\star_\eta(\eta)\dot{e}_a = M^\star_\eta(\eta)\ddot{\eta}_d - [-C^\star_\eta(v,\eta)\dot{\eta} - D^\star_\eta(v,\eta)\dot{\eta} \\ + \tau^\star_\eta(\eta) - g^\star_\eta(\eta) - \chi^\star_\eta(t)] + M^\star_\eta(\eta)\alpha_2 \dot{e} \tag{26}$$

Assumption 2: *The dynamics term $\chi^\star_\eta(t)$ in (8), which is considered as time-varying external disturbances (currents) combined with parametric uncertainties, is assumed to be a continuous Lipschitz function. Hence, its time derivative exists, and is bounded [5].*

Now, considering the vehicle dynamics linearity with respect to its dynamic parameters, we can express the terms (i.e., $\chi^\star_\eta(t)$ and $g^\star_\eta(\eta)$, previously explained in Section III), which definitely affect the vehicle's steady-state, as follows [28]:

$$\chi^\star_\eta(t) + g^\star_\eta(\eta) = \Phi_\vartheta \vartheta^T \tag{27}$$

Substituting the proposed SACT+ control law (22) as well as (27) into (26), yields:

$$M^\star_\eta(\eta)\dot{e}_a = M^\star_\eta(\eta)\ddot{\eta}_d - [-C^\star_\eta(v,\eta)\dot{\eta} - D^\star_\eta(v,\eta)\dot{\eta} \\ + (C^\star_\eta(v,\eta) + D^\star_\eta(v,\eta))(\dot{\eta}_d - \alpha_1\Lambda) + M^\star_\eta(\eta)(\ddot{\eta}_d + \overline{\tau}) \tag{28} \\ + \Phi_\vartheta \hat{\vartheta}^T - \Phi_\vartheta \vartheta^T] + M^\star_\eta(\eta)\alpha_2 \dot{e}$$

If we introduce $\tilde{\vartheta}$ as:

$$\tilde{\vartheta} = \hat{\vartheta} - \vartheta \tag{29}$$

Then, we can rewrite the resulting closed-loop error dynamics as follows:

$$M^\star_\eta(\eta)\dot{e}_a = -C^\star_\eta(v,\eta)\dot{e} - D^\star_\eta(v,\eta)\dot{e} + C^\star_\eta(v,\eta)\alpha_1\Lambda \\ + D^\star_\eta(v,\eta)\alpha_1\Lambda - M^\star_\eta(\eta)K_p(\cdot)e(t) - M^\star_\eta(\eta)K_d(\cdot)\dot{e}(t) \tag{30} \\ - \Phi_\vartheta \tilde{\vartheta}^T + M^\star_\eta(\eta)\alpha_2 \dot{e}$$

where $\overline{\tau}$ has been designed in (21).
To continue with this stability analysis, based on Lyapunov direct method, let us consider the following function as a Lyapunov candidate, $V : \mathbb{R}^{6\times6} \times \mathbb{R}^{6\times1} \to \mathbb{R}$:

$$V(r,\tilde{\vartheta}) = \frac{1}{2}e_a^T M^\star_\eta(\eta)e_a + \frac{1}{2}\tilde{\vartheta}^T \Gamma_\vartheta \tilde{\vartheta} + \frac{1}{2}\Lambda^T \Lambda + \frac{1}{2} \\ \times e^T \alpha_2[D^\star_\eta(v,\eta) - \alpha_2 M^\star_\eta(\eta)]e + \int_0^e \zeta^T M^\star_\eta(\eta)K_p(\zeta)d\zeta \\ + \int_0^e \zeta^T \alpha_2 M^\star_\eta(\eta)K_d(\zeta)d\zeta \tag{31}$$

which satisfies the following inequalities:

$$\kappa_1 \left[\|r\|^2 + \left\|\tilde{\vartheta}\right\|^2\right] \leq V(r,\tilde{\vartheta}) \leq \kappa_2 \left[\|r\|^2 + \left\|\tilde{\vartheta}\right\|^2\right] \tag{32}$$

where $\kappa_1 = \frac{1}{2}min\{1, K_1\}$, $\kappa_2 = \frac{1}{2}max\{1, K_2\}$, are positive constants and $r = [e_a^T, e^T, \dot{e}^T, \Lambda^T]^T$. K_1 and K_2 are given subsequently.

Remark 4: *The matrix $M^\star_\eta(\eta)$ is symmetric, bounded, and positive definite [5], that is, there exist $K_1 > 0$ and $K_2 > 0$ such that $M^\star_\eta(\eta)$ satisfies: $0 < K_1 I \leq M^\star_\eta(\eta) = M^\star_\eta(\eta)^T \leq K_2 I < \infty$. Where $I \in \mathbb{R}^{6\times6}$ is the identity matrix. Furthermore, the matrix $D^\star_\eta(v,\eta)$ satisfies $\eta^T D^\star_\eta(v,\eta)\eta > 0$, $\forall v, \eta \neq 0 \in \mathbb{R}^{6\times1}$[8].*

The proposed Lyapunov function candidate $V(r,\tilde{\vartheta})$ is positive definite and radially unbounded, based on the following propositions. The first, second, and third terms in the right-hand side (RHS) of (31) satisfy $e_a^T M^\star_\eta(\eta)e_a > 0$, $\tilde{\vartheta}^T \Gamma_\vartheta \tilde{\vartheta} > 0$, and $\Lambda^T \Lambda > 0$ respectively; since, $M^\star_\eta(\eta) > 0$ from *remark 4*, $\Gamma_\vartheta > 0$ by design, and identity matrix $I > 0$. Also, the matrix $[D^\star_\eta(v,\eta) - \alpha_2 M^\star_\eta(\eta)] > 0$ since α_2 is a positive design matrix subsequently in this proof. While the integral terms satisfy the following conditions [25]:

$$\int_0^e \zeta^T M^\star_\eta(\eta)K_p(\zeta)d\zeta > 0, \int_0^e \zeta^T M^\star_\eta(\eta)K_d(\zeta)d\zeta > 0, \\ \forall e \neq 0 \in \mathbb{R}^n \tag{33}$$

where $K_p(\zeta) > 0, K_d(\zeta) > 0$ by design (from (21)), which implies that $[M^\star_\eta(\eta)K_p(\zeta)] > 0, [M^\star_\eta(\eta)K_d(\zeta)] > 0$ (see [33]). From the arguments (33), we can deduce that:

$$\int_0^e \zeta^T M^\star_\eta(\eta)K_p(\zeta)d\zeta \to \infty, \text{ and} \\ \int_0^e \zeta^T M^\star_\eta(\eta)K_d(\zeta)d\zeta \to \infty \text{ as } \|e\| \to \infty \tag{34}$$

Next, the time derivative of $V(r,\tilde{\vartheta})$ evaluated along the trajectory of (30) can be written as follows:

$$\dot{V}(r,\tilde{\vartheta}) = e_a^T M^\star_\eta(\eta)\dot{e}_a + \frac{1}{2}e_a^T \dot{M}^\star_\eta(\eta)e_a + \tilde{\vartheta}^T \Gamma_\vartheta \dot{\tilde{\vartheta}} \\ + \Lambda^T \dot{\Lambda} + e^T \alpha_2[D^\star_\eta(v,\eta) - \alpha_2 M^\star_\eta(\eta)]\dot{e} + \frac{1}{2}e^T \alpha_2[-\alpha_2 \tag{35} \\ \times \dot{M}^\star_\eta(\eta)]e + e^T M^\star_\eta(\eta)K_p(\cdot)\dot{e} + e^T \alpha_2 M^\star_\eta(\eta)K_d(\cdot)\dot{e}$$

This article has been accepted for publication in IEEE Transactions on Systems, Man, and Cybernetics: Systems. This is the author's version which has not been fully edited and content may change prior to final publication. Citation information: DOI 10.1109/TSMC.2024.3412797

7

Consequently, substituting the resulting vehicle's closed-loop dynamics (30), the saturation-based dynamic mechanism (23), and the adaptation dynamics (24) into (35) leads to:

$$
\begin{aligned}
\dot{V}(r,\tilde{\vartheta}) = & \dot{e}^T \left[\frac{1}{2}\dot{M}_\eta^\star(\eta) - C_\eta^\star(v,\eta) \right] \dot{e} + [\dot{e}^T \alpha_1 \Lambda - e^T \alpha_2 \dot{e} \\
& + e^T \alpha_1 \alpha_2 \Lambda] C_\eta^\star(v,\eta) - \dot{e}^T \dot{M}_\eta^\star(\eta)\alpha_2 e - \dot{e}^T D_\eta^\star(v,\eta)\dot{e} \\
& - \dot{e}^T M_\eta^\star(\eta)K_d(\cdot)\dot{e} - e^T \alpha_2 M_\eta^\star(\eta)K_p(\cdot)e - \Lambda^T \Lambda \\
& - \Lambda^T K_p(\cdot)e - \Lambda^T K_d(\cdot)\dot{e} + \dot{e}^T M_\eta^\star(\eta)\alpha_2 \dot{e} \\
& + \dot{e}^T D_\eta^\star(v,\eta)\alpha_1 \Lambda + e^T \alpha_2 D_\eta^\star(v,\eta)\alpha_1 \Lambda
\end{aligned} \quad (36)
$$

Even though the Coriolis and centripetal forces effect can be compensated by the saturation-based dynamic mechanism in the proposed SACT+ control law (22), in most of the control schemes proposed for underwater vehicles including our prototype vehicle, the following assumption is often considered.

Assumption 3: *In real-time applications, the Coriolis and centripetal forces effect is often neglected based on the assumption that the vehicle moves slowly [5].*

Then based on *assumption 3* and the property $\dot{e}^T[\frac{1}{2}\dot{M}_\eta^\star(\eta) - C_\eta^\star(v,\eta)]\dot{e} = 0$ (see [8], for further details), (36) can be simplified and rewritten as follows:

$$
\begin{aligned}
\dot{V}(r,\tilde{\vartheta}) = & -\dot{e}^T D_\eta^\star(v,\eta)\dot{e} - \Lambda^T \Lambda - \dot{e}^T [M_\eta^\star(\eta)K_d(\cdot) \\
& - \alpha_2 M_\eta^\star(\eta)]\dot{e} - e^T \alpha_2 M_\eta^\star(\eta)K_p(\cdot)e - \Lambda^T [K_d(\cdot) \\
& - \alpha_1 D_\eta^\star(v,\eta)]\dot{e} - \Lambda^T [K_p(\cdot) - \alpha_1 \alpha_2 D_\eta^\star(v,\eta)]e
\end{aligned} \quad (37)
$$

Using Young's inequality, $\dot{V}(r,\tilde{\vartheta})$ can be upper-bounded and simplified further as follows:

$$
\begin{aligned}
\dot{V}(r,\tilde{\vartheta}) \leq & -\dot{e}^T D_\eta^\star(v,\eta)\dot{e} - \Lambda^T \Lambda - \dot{e}^T [K_{d\min} - \alpha_2] \\
& \times M_\eta^\star(\eta)\dot{e} - e^T \alpha_2 [M_\eta^\star(\eta)K_{p\min}]e - \frac{1}{2} \\
& \times \left[K_{p\min}^\star + K_{d\min}^\star - \alpha_{1i}D_{\eta i}^\star(v,\eta)(1+\alpha_{2i}) \right] \|r\|^2
\end{aligned} \quad (38)
$$

Based on (38) above, we can deduce that $\dot{V}(r,\tilde{\vartheta})$ is negative semidefinite when α_{1i} and α_{2i} are properly designed as follows:

$$
\alpha_{1i} < \frac{K_{p\min}^\star + K_{d\min}^\star}{D_{\eta i}^\star(v,\eta)[1+\alpha_{2i}]} \text{ and } \alpha_{2i} < K_{d\min}^\star, i = \overline{1,6} \quad (39)
$$

As long as (39) is satisfied, $\dot{V}(r,\tilde{\vartheta})$ is negative semidefinite from (38), while $V(r,\tilde{\vartheta})$ in (31) is uniformly continuous, positive definite, and radially unbounded, this implies that the origin of the resulting closed-loop dynamics (30) is stable through invoking Barbalat's Lemma [28]. This also implies that $V(r,\tilde{\vartheta})$ is bounded. Hence, r, e_a, $\dot{e}$, and e are all bounded. Similarly, the integral of $\hat{\vartheta}$ and Λ are bounded since they both depend on $\dot{e}$ and e.

Remark 5: *Note that the tracking error can only stay around the origin but not at the origin precisely due to many factors. Such factors are the measurement noise from the vehicle's sensors, the inherent uncertainties of the vehicle combined with external disturbances from the marine environment, etc.*

Remark 6: *It is worth noting that **Algorithm 1** is designed in the forthcoming section to ensure that (39) is satisfied in both theory and experiment.*
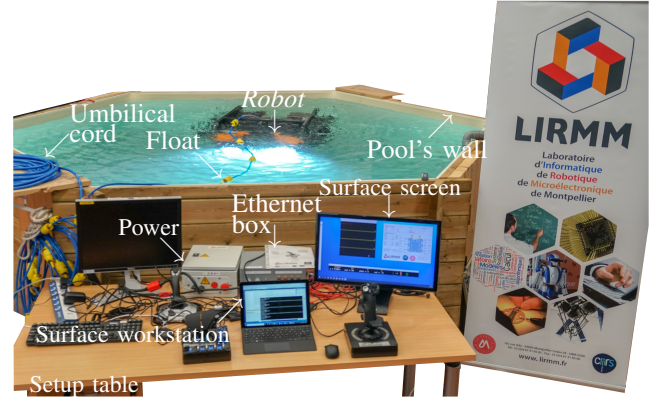

Fig. 3. The experimental setup main components: underwater robot, surface workstation, testing pool, and power supply.

V. OBTAINED EXPERIMENTAL RESULTS

A. Control Implementation Issues

Although the proposed SACT+ scheme design and its stability analysis are addressed for all the vehicle's degrees of freedom in Sections III and IV, the real-time experiments focus on controlling two degrees of freedom, *namely the depth and the yaw motions*. An in-depth study is conducted experimentally on these two degrees of freedom without the loss of generality. It is worth noting that from the practical perspective, the noisy measurement from the depth sensor (for measuring the depth (z)) and the sensitivity of the yaw (ψ) make these two degrees of freedom challenging to control, especially for low-cost vehicles which lack expensive sensors such as our vehicle. Furthermore, the surge (x) and the sway (y) motions of the vehicle are not measurable in the real-time tests, while the roll (ϕ) and the pitch (θ) are passively stable. Also, in many applications, the vehicle is needed to be operated at $\phi \approx \theta \approx 0°$, and on many commercial ATUVs these degrees of freedom are passively stable [11]. The proposed control scheme is implemented on the robot in our testing pool for a real-time validation, as shown in the experimental setup (i.e., Fig. 3). A computer with Intel Core i7-3520M 2.9 GHz CPU, 32 GB of RAM, and Windows 11 as an OS is used to compute the proposed control law written in Visual C++. The computation of the proposed control law in real-time is based on the measurements from the vehicle's sensors (i.e., depth sensor and inertial measurement unit (IMU)), then sent to the actuators of the vehicle.

B. Proposed Validation Scenarios

To evaluate the efficacy and robustness of the proposed SACT+ controller against the classical CT and IFC (in [22]) from the literature, three different scenarios have been proposed for the real-time experimental tests, as follows:

1) Scenario 1 (Nominal Case): The aim of this experiment is to tune online the gains of each controller. During this process, the vehicle tracks the desired trajectory in the presence of internal perturbations only, such as sensor noise and modeling errors. Then, the controller gains, producing the best tracking, are used in the subsequent scenarios to assess the controller's efficiency and robustness.

This article has been accepted for publication in IEEE Transactions on Systems, Man, and Cybernetics: Systems. This is the author's version which has not been fully edited and content may change prior to final publication. Citation information: DOI 10.1109/TSMC.2024.3412797

8

2) Scenario 2 (Robustness Test): This scenario investigates the robustness of each controller toward parametric uncertainties such as variations in damping/buoyancy of the vehicle.

3) Scenario 3 (External Disturbance Rejection): In this experiment, we propose to investigate the robustness of the controllers in handling both anticipated and unanticipated external disturbances in real-life marine applications. These situations may include strong mechanical impacts, collisions with massive marine structures and animals, manipulations of tools and samples, and strong time-varying effects (currents and waves). Then, the capacity of each controller to keep the vehicle in the vicinity of the desired trajectory is assessed.

C. Experimental Results Obtained From Real-time Scenarios

To demonstrate the superior performance of the proposed SACT+ scheme compared to CT and IFC techniques from the literature, as well as to validate the conditions in Theorem 1, we tested in real-time the following scenarios:

1) Experimental results of Scenario 1: In this experiment, the *Leonard* vehicle should follow the desired time-varying depth and yaw trajectories simultaneously. Concerning the depth test, the vehicle moves vertically downwards to a depth of $0.3\,\text{m}$ from the water surface and remains at this position for about $13\,\text{s}$. Then, it moves vertically upwards by $0.1\,\text{m}$ within about $8\,\text{s}$ and stays there until the end of this test. Similarly, for the yaw tracking, the vehicle turns from its initial yaw to the desired yaw of $+60°$ within just $9\,\text{s}$. Then, it maintains this orientation for $13\,\text{s}$. Finally, the vehicle changes its yaw orientation from $+60°$ to $-60°$ in $9\,\text{s}$ and maintains this heading until the end of the test. It is worth noting that, in this test neither parametric uncertainties nor external disturbances are considered.

The obtained control design parameters are summarized in TABLE II; each of these parameters is tuned using Algorithm 1. For robustness test purposes, these parameters remain unchanged throughout the forthcoming scenarios. Even though the vehicle tracks the desired depth and yaw in nominal condition, the tether force keeps disturbing the vehicle during this test due to its non negligible stiffness. This is the main reason why, some slight depth tracking errors are noticed for the case of both CT (more pronounced) and IFC; however, the proposed SACT+ controller compensates for this effect, as can be seen in Fig. 4 (top left plot).

We can also observe, from the top right plot of Fig. 4, some slight yaw tracking errors for CT and IFC, which are resulted from the coupling effect induced by the inability of these controllers to suppress the tether's force affecting the depth tracking. Besides the experiment proves better tracking performance of the proposed SACT+ scheme. This inference can be confirmed from Fig. 4 (middle plots), as well as from the performance index (root mean square error RMSE) summarized in TABLE III and obtained by using $RMS[e(t)]_{position/attitude} = [\frac{1}{T_f}\int_0^{T_f}\|e(t)\|^2 dt]^{\frac{1}{2}}$, where $e(t)$ is the tracking error and T_f is the test duration.

The evolution of the control inputs and compensation/adaptation parameters is shown in Fig. 4 (bottom plots) and Fig. 5 (left plots), respectively. The compensation/adaptation parameters are generated online by the

TABLE II
PROPOSED SACT+ CONTROL PARAMETERS USED IN REAL-TIME EXPERIMENTS

Depth	$\bar{s}_{p3} = 0.088$	$d_{p3} = 0.035$	$\delta_{p3} = 0.210$	$\alpha_{13} = 0.095$
	$\gamma_3 = 1.000$	$\bar{s}_{d3} = 0.001$	$d_{d3} = 0.310$	$\delta_{d3} = 0.500$
	$\alpha_{23} = 0.100$	$\Lambda_3(0) = 0.000$	$\hat{\vartheta}_d(0) = 0.000$	
Yaw	$\bar{s}_{p6} = 6.210$	$d_{p6} = 0.040$	$\delta_{p6} = 0.700$	$\alpha_{16} = 0.001$
	$\gamma_6 = 0.000$	$\bar{s}_{d6} = 0.150$	$d_{d6} = 0.020$	$\delta_{d6} = 0.400$
	$\alpha_{26} = 0.000$	$\Lambda_6(0) = 0.000$		

TABLE III
INDICES REPRESENTING THE TRACKING PERFORMANCE (RMSE) AND INTEGRAL OF CONTROL INPUTS (INT) FOR THE CONTROLLERS

Index	Scenario	CT [31]	IFC [22]	SACT+
RMSE$_{depth}$ $[\times 10^{-2}\,\text{m}]$	S1	5.3453	0.4370	0.3954
	S2	5.7571	10.9150	0.9908
	S3	–	–	3.4329
RMSE$_{yaw}$ $[\times 10^{-2}\,\text{deg}]$	S1	3.8107	6.8689	1.4833
	S2	10.1676	13.7463	0.8708
	S3	–	–	4.4333
INT$_{depth}$	S1	175.3066	153.1951	119.3895
	S2	62.9238	437.7868	56.3791
	S3	–	–	146.8001
INT$_{yaw}$	S1	7.7351	15.2688	8.9263
	S2	6.8429	10.9387	1.5971
	S3	–	–	16.1717

proposed controller and included inside the control inputs producing the tracking performances in Fig. 4 (top plots). Therefore, the estimated adaptive ($\hat{\vartheta}_{d_{S1}}$) and compensation ($\Lambda_{d_{S1}}$) parameters converge to a steady state at each segment of the present test, as depicted in Fig. 5 (top and bottom left plots). Furthermore, the compensation ($\Lambda_{\psi_{S1}}$) parameter moves slightly to neutralize the high uncertainties due to the hydrodynamic and tether's force effects on the yaw, as shown in Fig. 5 (middle left plots). One can also notice that the SACT+ controller consumes less energy compared to the remaining controllers (from the literature) during the depth tracking, as shown in Fig. 4 (bottom left plot). To emphasize a trade-off between better performance and estimated energy consumption, we compute the integral of the control input index (INT), as $INT[\tau]_{position/attitude} = \int_{t_i}^{t_f}\|\tau(t)\|^2 dt$ with $\tau(t)$ denotes the vector of control inputs, t_i is initial time as the vehicle converges to the desired trajectory, and t_f stands for the final test time for each controller. The obtained results are presented in TABLE III. Also, from the same TABLE III, we can numerically deduce that the proposed SACT+ controller consumes approximately the same energy as the CT scheme from the literature for the yaw tracking in this scenario.

Remark 7: *It is worth mentioning the vehicle's initial conditions are far from the desired trajectory, which leads to high energy consumption in this test (see TABLE III).*

The proposed SACT+ design parameters can be tuned based on **Algorithm 1**.

2) Experimental results of Scenario 2: We introduce parametric uncertainties in the vehicle dynamics by modifying the terms $D_\eta^\star(\cdot)$ and $g_\eta^\star(\cdot)$ to $D_\eta^\star(\cdot)+\Delta D_\eta(\cdot)$ and $g_\eta^\star(\cdot)+\Delta g_\eta(\cdot)$, respectively, as follows. A rigid plastic sheet of size $0.45\,\text{m} \times 0.1\,\text{m}$ has been mounted at the vehicle's aft-most part, as illustrated in Fig. 6. This increases the rotational drag along

This article has been accepted for publication in IEEE Transactions on Systems, Man, and Cybernetics: Systems. This is the author's version which has not been fully edited and content may change prior to final publication. Citation information: DOI 10.1109/TSMC.2024.3412797
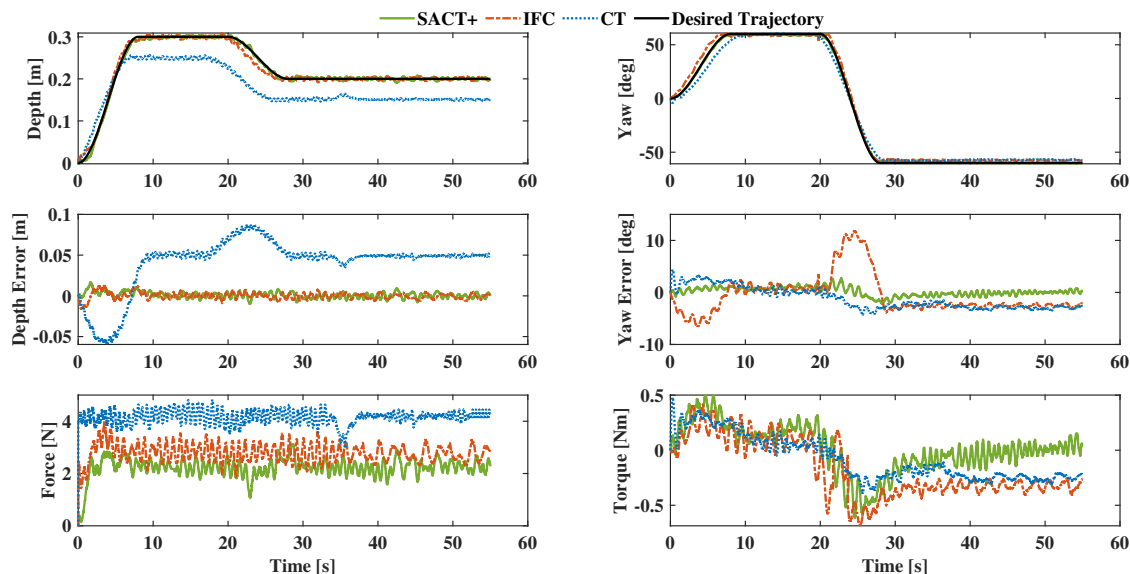
9

Fig. 4. Tracking performance of the proposed SACT+ scheme compared with both CT and IFC controllers implemented on *Leonard* vehicle in real-time nominal case: (top plots) depth and yaw trackings, (middle plots) depth and yaw corresponding tracking errors and (bottom plots) display the evolution of the vehicle's control inputs.
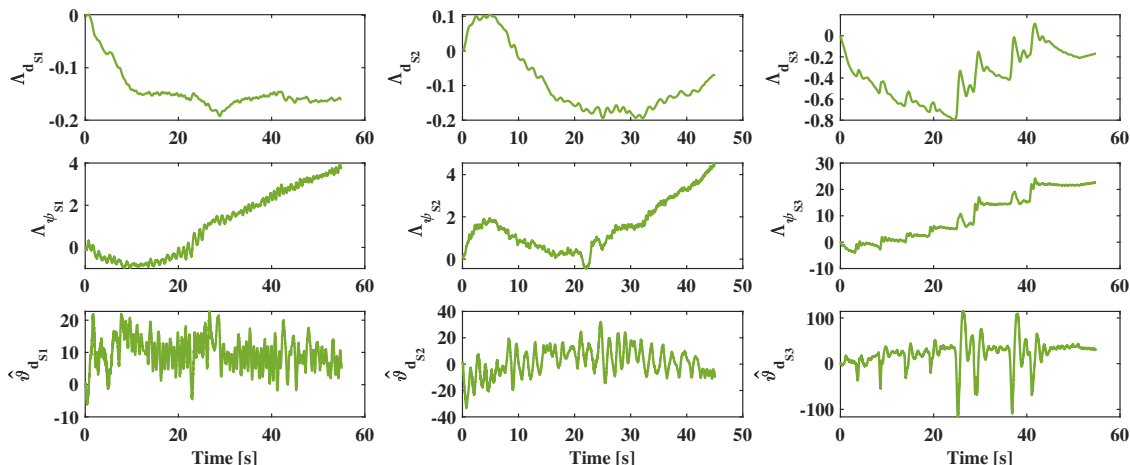

Fig. 5. Evolution versus time of compensation and adaptation parameters: (left plots) parameters for Scenario 1, (middle plots) parameters for Scenario 2, and (right plots) parameters for Scenario 3.

the yaw, which implies an increased $D_\eta^\star(\cdot)$ term by $\Delta D_\eta(\cdot) = +90\%$ w.r.t its nominal value. Similarly, the $g_\eta^\star(\cdot)$ term has been changed to $g_\eta^\star(\cdot) + \Delta g_\eta(\cdot)$ (with $\Delta g_\eta(\cdot) = +100\%$ w.r.t its nominal value), by attaching two floats on both sides of the vehicle (Fig. 6). The modified vehicle is controlled to follow similar reference trajectories as in the nominal case.

The obtained results are depicted in Fig. 7 (top plots). The parametric uncertainties introduce tracking offsets in all the degrees of freedom for both CT and IFC controllers. Indeed, the controlled output of the CT scheme exhibits some oscillations towards the end of the experiment when the controller attempts to compensate for the effects of the parametric uncertainties. For the case of the IFC method, the controller shows a stable behavior at the beginning of this test. Additionally, underwater environments are well known for many

uncertainties, such as temperature changes, pressure variations, and so on. Therefore, the IFC scheme oscillates slightly around the desired depth. This behavior triggers the aggressive action of the IFC scheme while trying to maintain the vehicle around the desired depth. As a result, the controller sends higher control inputs to the three thrusters used to manipulate the vehicle along the depth axis. Based on this unstable behavior of the IFC scheme, under critical uncertainty conditions, for the case of depth tracking, the security system of the vehicle shut down all the thrusters for safety reasons. Hence, the test for this controller was stopped automatically, and the vehicle surfaced after 18 s, approximately as shown in Fig. 7. In contrast, the proposed SACT+ scheme proves its effectiveness and robustness by keeping the vehicle approximately on the desired trajectories. However, the controller takes about 2 s

This article has been accepted for publication in IEEE Transactions on Systems, Man, and Cybernetics: Systems. This is the author's version which has not been fully edited and content may change prior to final publication. Citation information: DOI 10.1109/TSMC.2024.3412797

10

Algorithm 1 Proposed Controller's Parameters Tuning

Inputs: $max\{|e_i|\}$, $max\{|\dot{e}_i|\}$
Outputs: d_{pi}, d_{di}, $\bar{s}_{pi}$, $\bar{s}_{di}$, δ_{di}, δ_{pi}, α_{1i}, α_{2i}, and γ_i

1: Design the saturation bound d_{pi} with its linear region in the interval $[-d_{pi}, d_{pi}]$
2: $d_{pi} = 50\% \times max\{|e_i|\}$
3: **while** $d_{di} = \bar{s}_{di} = \delta_{di} = \delta_{pi} = \alpha_{1i} = \alpha_{2i} = 0$ **do**
4: $\quad \bar{s}_{pi}++$ {keep increasing $\bar{s}_{pi}$ until the closed-loop system trajectory is closed to the desired one}
5: **end while**
6: $d_{di} = 50\% \times max\{|\dot{e}_i|\}$
7: $\bar{s}_{di}++$ {to smooth undesirable oscillations}
8: Design δ_{pi} within $[0,1]$
9: Select $\delta_{di} \geq \delta_{pi}$ also within $[0,1]$
10: Design $\alpha_{1i} > 0, \alpha_{2i} > 0$ {hint: $\alpha_{1i} < 50\% \times [\bar{s}_{pi} + \bar{s}_{di}]$ and $\alpha_{2i} < 50\% \times [\bar{s}_{di}]$}
11: Fine-tune $\delta_{di}, \delta_{pi}, \alpha_{1i}, \alpha_{2i}$ {to improve performance}
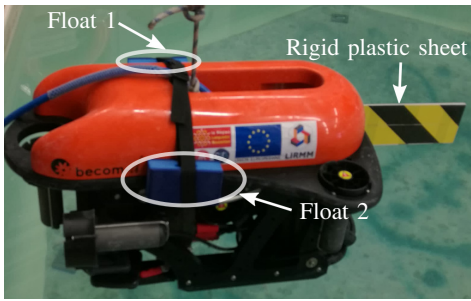12: Design $\gamma_i > 0$ {note that γ_i is the adaptation rate}

Fig. 6. Illustration of a temporary reconfiguration of the vehicle to introduce parametric uncertainties: each float changes the vehicle buoyancy by $+50\%$, while the rigid plastic sheet increases the rotational drag on the yaw by $+90\%$.

to deal with the uncertainty on depth. The tracking errors of all the controllers are shown in Fig. 7 (middle plots), and their numerical values in terms of RMS are summarized in TABLE III. We also observe that the proposed controller consumes less energy when compared to the other tested controllers from the literature. This claim can also be confirmed from both TABLE III and Fig. 7 (bottom plots). Similar to the previous scenario, the evolution of the compensation and adaptation parameters is shown in Fig. 5 (middle plots). We can effectively notice the dynamic changes of these parameters of the proposed SACT+ scheme in response to neutralize the negative effects of the introduced uncertainties. It is worth mentioning that the performance of the majority of the existing control schemes, from the literature, degraded in this scenario without readjusting their parameters for comparison purposes. Contrary to the proposed SACT+ scheme, in this paper, where the same numerical values of the control parameters are used for all the experimental tests.

Remark 8: In this scenario, we considered neglecting $C_{\eta}^{\star}(\cdot)$ term, based on assumption 2.

3) Experimental results Scenario 3: To evaluate the proposed SACT+ control scheme towards both expected and unexpected external disturbances in real-time, we set up this scenario using successive external pushes on the vehicle. We consider the same intensity for each push, which is approximated as a force equivalent to about 25% of the vehicle's weight. Then, the external push is applied to the vehicle's body using a stick affecting both the depth and yaw axes when the vehicle is tracking the desired trajectories (as illustrated in Fig. 8). We apply this external push on the depth six times. The application points are $0.18\,\mathrm{m}$ (a'), $0.3\,\mathrm{m}$ (b'_1 and b'_2), $0.25\,\mathrm{m}$ (c') and $0.2\,\mathrm{m}$ (d'_1 and d'_2), which correspond to different positions of the vehicle moving vertically downwards, stabilizing at an intermediate position, moving vertically upwards and hovering at final depth, respectively (see top left plot of Fig. 9). The proposed SACT+ controller rejects all the six disturbances and stabilizes the vehicle within about $2\,\mathrm{s}$. Moreover, the dynamic coupling of this external push reproduces an effect on the yaw axis, which can be traced using the dash-dash lines as depicted in Fig. 9 (right plots).

To further rechallenge the proposed SACT+ scheme, we applied approximately the same push on the yaw axis two times, that is, at e'_1 and e'_2. Also, the proposed controller rejected the external pushes and kept the vehicle around the desired yaw for a finite time (about $2\,\mathrm{s}$). However, slightly higher coupling effects are observed compared to the case of the push applied to the depth axis only. This can be noticed by using dotted lines as depicted in Fig. 9 (left plots). It is worth to note that, there is always a trade-off between the tracking performance and vehicle's energy consumption. The middle plots of Fig. 9 display the tracking errors of both depth and yaw motions, while the corresponding control inputs are depicted in the lower plots of the same figure. Furthermore, the evolution of the compensation/adaptation parameters is shown in Fig. 5 (right plots). In the same figure, we can notice how the external pushes affect the behavior of the compensation and adaptation laws of the proposed SACT+ controller. Finally, the numerical values of the performance indices of the proposed SACT+, in this test, are summarized in Table III.

Remark 9: Note that, we only validated the proposed SACT+ controller in real-time for the case of Scenario 3 to rechallenge the controller. Indeed, for a fair comparison, we need to apply the same external disturbances for all the controllers under the same conditions (time, application point, direction, magnitude, etc.), which is too difficult experimentally. An illustrated video of all the obtained real-time experimental results is available at: **https : //youtu.be/RhjoPX4rKgQ**

VI. CONCLUSION AND FUTURE WORK

In this work, a SACT+ control scheme has been proposed for underwater vehicles. Lyapunov analysis has been conducted to prove that the resulting closed-loop dynamics is stable. Then, the proposed SACT+ scheme has been implemented on *Leonard* underwater vehicle for trajectory tracking tasks. Besides rigorous scenario-based experimental tests of the proposed SACT+ scheme, comparative studies with two other controllers from the literature have been conducted. The obtained results demonstrate clearly the robustness and effectiveness of the proposed SACT+ control approach in different operating conditions, including external disturbances, parametric uncertainties, sensors' noise, as well as the unpredictable nature of underwater environments. The proposed
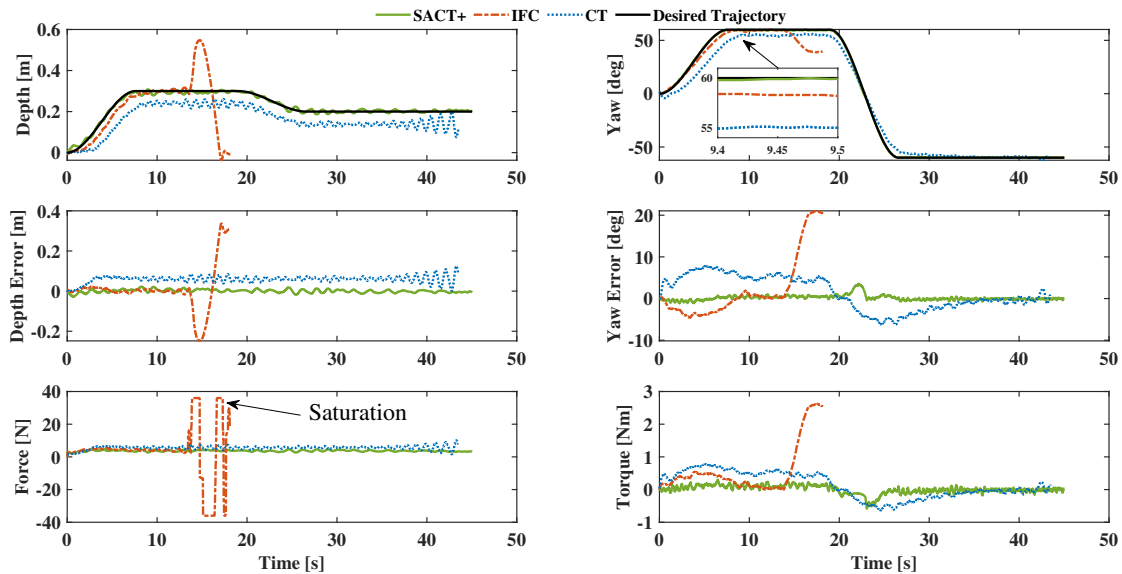
Fig. 7. Robustness comparison of the proposed SACT+, CT, and IFC controllers towards parametric uncertainties considered on the real vehicle. In this experiment, the $D_\eta^\star(\cdot)$ and $g_\eta^\star(\cdot)$ terms of the vehicle have been changed by $\Delta D_\eta(\cdot) = +90\%$ and $\Delta g_\eta(\cdot) = +100\%$, respectively: (top plots) depth and yaw trackings, (middle plots) depth and yaw tracking errors, and (bottom plots) the vehicle's control inputs versus time.
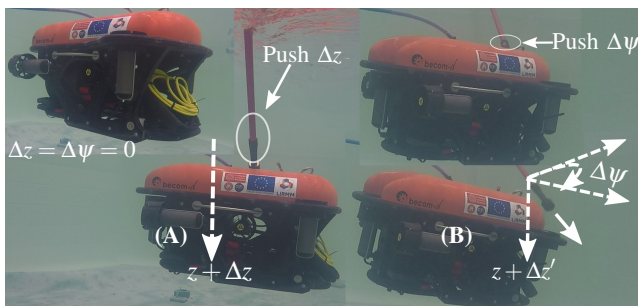

Fig. 8. Illustration of the *Scenario* 3 in a real-time experiment: (A) external push (Δz) applied along depth axis, which force is approximately equivalent to 25% of the vehicle's total weight. (B) A similar external push ($\Delta \psi$) is applied on yaw, with its coupling effect ($\Delta z'$) on depth. The perturbation on depth may also cause an effect on yaw ($\Delta \psi'$), due to the dynamic coupling.

SACT+ control scheme demonstrated nice performance for the control of underwater vehicles. However, integrating a high-gain observer into the proposed SACT+ scheme, for external disturbance and velocity estimations, should improve its performance and will be a part of our future works.

REFERENCES

[1] P. A. Lusty and B. J. Murton, "Deep-ocean mineral deposits: metal resources and windows into earth processes," *Elements*, vol. 14, no. 5, pp. 301–306, 2018.

[2] M. J. Er, H. Gong, Y. Liu, and T. Liu, "Intelligent trajectory tracking and formation control of underactuated autonomous underwater vehicles: A critical review," *IEEE Transactions on Systems, Man, and Cybernetics: Systems*, vol. 54, no. 1, pp. 543–555, 2024.

[3] N. Gu, D. Wang, Z. Peng, J. Wang, and Q.-L. Han, "Disturbance observers and extended state observers for marine vehicles: A survey," *Control Engineering Practice*, vol. 123, p. 105158, 2022.

[4] H. Bao, Y. Wang, H. Zhu, X. Li, and F. Yu, "Numerical and experimental analysis of motion control of offshore fishing unmanned underwater vehicle in ocean environment," *Ocean Engineering*, vol. 295, p. 116886, 2024.

[5] A. S. Tijjani, A. Chemori, and V. Creuze, "Robust adaptive tracking control of underwater vehicles: Design, stability analysis, and experiments," *IEEE/ASME Transactions on Mechatronics*, vol. 26, no. 2, pp. 897–907, 2021.

[6] B. L. Gupta, *Autonomous Underwater Vehicles: Global Markets to 2022*. BCC Research, 2018.

[7] Z. M. Li and J. H. Park, "Dissipative fuzzy tracking control for nonlinear networked systems with quantization," *IEEE Transactions on Systems, Man, and Cybernetics: Systems*, vol. 50, no. 12, pp. 5130–5141, 2020.

[8] A. S. Tijjani, A. Chemori, S. A. Ali, and V. Creuze, "Continuous–discrete observation-based robust tracking control of underwater vehicles: Design, stability analysis, and experiments," *IEEE Transactions on Control Systems Technology*, vol. 31, no. 4, pp. 1477–1492, 2023.

[9] J. Zhang, X. Xiang, W. Li, and Q. Zhang, "Adaptive saturated path following control of underactuated auv with unmodeled dynamics and unknown actuator hysteresis," *IEEE Transactions on Systems, Man, and Cybernetics: Systems*, vol. 53, no. 10, pp. 6018–6030, 2023.

[10] C. Zhao and L. Guo, "Control of nonlinear uncertain systems by extended pid," *IEEE Transactions on Automatic Control*, pp. 1–1, 2020.

[11] A. S. Tijjani, A. Chemori, and V. Creuze, "A survey on tracking control of unmanned underwater vehicles: Experiments-based approach," *Annual Reviews in Control*, vol. 54, pp. 125–147, 2022.

[12] Q. Wang, Z. G. Wu, P. Shi, H. Yan, and Y. Chen, "Stability analysis and control for switched system with bounded actuators," *IEEE Transactions on Systems, Man, and Cybernetics: Systems*, vol. 50, no. 11, pp. 4506–4512, 2020.

[13] Z. A. Ali, X. Li, and M. A. Tanveer, "Controlling and stabilizing the position of remotely operated underwater vehicle equipped with a gripper," *Wireless Personal Communications*, pp. 1–16, 2019.

[14] M. Muscat, A. Cammarata, P. D. Maddio, and R. Sinatra, "Design and development of a towfish to monitor marine pollution," *Euro-Mediterranean Journal for Environmental Integration*, vol. 3, no. 1, p. 11, 2018.

[15] W. Liu, X. Ding, J. Wan, R. Nian, B. He, Y. Shen, and T. Yan, "An effective motion control based on 2-dof pid and elm for auv," in *OCEANS 2018 MTS/IEEE Charleston*, pp. 1–4, IEEE, 2018.

[16] H. Wu, S. Song, K. You, and C. Wu, "Depth control of model-free auvs via reinforcement learning," *IEEE Transactions on Systems, Man, and Cybernetics: Systems*, vol. 49, no. 12, pp. 2499–2510, 2019.

[17] R. Cui, C. Yang, Y. Li, and S. Sharma, "Adaptive neural network control of auvs with control input nonlinearities using reinforcement learning," *IEEE Transactions on Systems, Man, and Cybernetics: Systems*, vol. 47, no. 6, pp. 1019–1029, 2017.

[18] I. Carlucho, M. De Paula, S. Wang, Y. Petillot, and G. G. Acosta, "Adaptive low-level control of autonomous underwater vehicles using deep
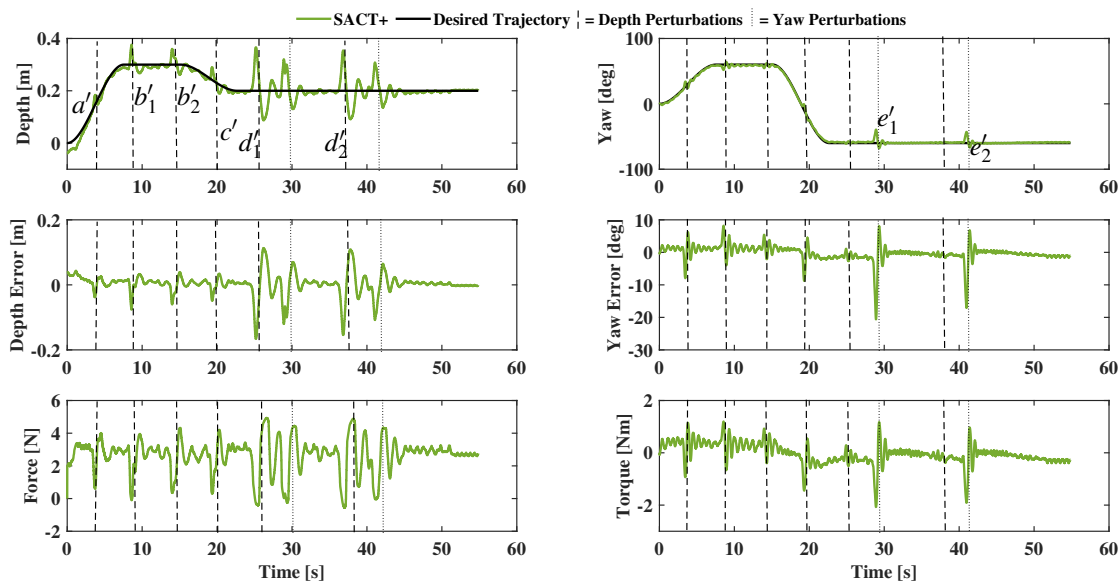
Fig. 9. External disturbance rejection of the proposed SACT+ controller towards external push: (top plots) robustness of the controller in rejecting successive external pushes applied on both the depth and yaw axes during the desired trajectory tracking task, (middle plots) the corresponding tracking errors of the depth and yaw, and (bottom plots) generated control inputs evolution versus time.

reinforcement learning," *Robotics and Autonomous Systems*, vol. 107, pp. 71–86, 2018.

[19] M. L. Greene, Z. I. Bell, S. Nivison, and W. E. Dixon, "Deep neural network-based approximate optimal tracking for unknown nonlinear systems," *IEEE Transactions on Automatic Control*, vol. 68, no. 5, pp. 3171–3177, 2023.

[20] X. Wang, B. Xu, and Y. Guo, "Fuzzy logic system-based robust adaptive control of auv with target tracking," *International Journal of Fuzzy Systems*, vol. 25, no. 1, pp. 338–346, 2023.

[21] X. Wang, "Active fault tolerant control for unmanned underwater vehicle with sensor faults," *IEEE Transactions on Instrumentation and Measurement*, vol. 69, no. 12, pp. 9485–9495, 2020.

[22] X. Xiang, C. Yu, and Q. Zhang, "Robust fuzzy 3d path following for autonomous underwater vehicle subject to uncertainties," *Computers & Operations Research*, vol. 84, pp. 165–177, 2017.

[23] A. Manzanilla, P. Castillo, and R. Lozano, "Nonlinear algorithm with adaptive properties to stabilize an underwater vehicle: real-time experiments," *IFAC-PapersOnLine*, vol. 50, no. 1, pp. 6857–6862, 2017.

[24] W. Shang and S. Cong, "Nonlinear computed torque control for a high-speed planar parallel manipulator," *Mechatronics*, vol. 19, no. 6, pp. 987–992, 2009.

[25] E. Campos, A. Chemori, V. Creuze, J. Torres, and R. Lozano, "Saturation based nonlinear depth and yaw control of underwater vehicles with stability analysis and real-time experiments," *Mechatronics*, vol. 45, pp. 49–59, 2017.

[26] Y. Chen, K. Wang, and W. Chen, "Adaptive fuzzy depth control with trajectory feedforward compensator for autonomous underwater vehicles," *Advances in Mechanical Engineering*, vol. 11, no. 3, p. 1687814019838172, 2019.

[27] Y. Chen, R. Zhang, X. Zhao, and J. Gao, "Adaptive fuzzy inverse trajectory tracking control of underactuated underwater vehicle with uncertainties," *Ocean engineering*, vol. 121, pp. 123–133, 2016.

[28] G. Antonelli, S. Chiaverini, N. Sarkar, and M. West, "Adaptive control of an autonomous underwater vehicle: experimental results on odin," *IEEE Transactions on Control Systems Technology*, vol. 9, no. 5, pp. 756–765, 2001.

[29] T. Yang, N. Sun, and Y. Fang, "Adaptive fuzzy control for uncertain mechatronic systems with state estimation and input nonlinearities," *IEEE Transactions on Industrial Informatics*, vol. 18, no. 3, pp. 1770–1780, 2022.

[30] A. R. Chowdhury, V. Vishwanathan, B. Prasad, R. Kumar, and S. K. Panda, "Inverse dynamics control of a bio-inspired robotic-fish underwater vehicle propulsion based on lighthill slender body theory," in *OCEANS 2014 - TAIPEI*, pp. 1–6, 2014.

[31] S. C. Martin and L. L. Whitcomb, "Preliminary experiments in fully actuated model based control with six degree-of-freedom coupled dynamical plant models for underwater vehicles," in *2013 IEEE International Conference on Robotics and Automation*, pp. 4621–4628, 2013.

[32] Z. Huang, Z. Su, B. Huang, S. Song, and J. Li, "Quaternion-based finite-time fault-tolerant trajectory tracking control for autonomous underwater vehicle without unwinding," *ISA Transactions*, vol. 131, pp. 15–30, 2022.

[33] E. De Klerk, *Aspects of semidefinite programming: interior point algorithms and selected applications*, vol. 65. Springer Science & Business Media, 2006.

Auwal Shehu Tijjani obtained his M.ENG. degree in Mechatronic and Automatic Control from Universiti Teknologi Malaysia, Malaysia, in 2016. Then, he received his Ph.D. in Marine Robotics (Automatic Control) from LIRMM-CNRS, University of Montpellier, France, in 2021. He has been a Research Fellow and a Research Engineer with LAMIH-CNRS and French aerial drone company in 2022 and 2023, respectively. He is currently with CERI Digital Systems, IMT-Nord-Europe, Lille, France. His research focuses on advanced estimation and control for mobile robots, marine vehicles, and aerial drones.

Ahmed CHEMORI received both his M.Sc. and Ph.D. degrees in the field of Automatic Control from the Grenoble Institute of Technology, France, in 2001 and 2005, respectively. In 2006, he has been a fixed-term Postdoctoral Researcher at Automatic Control Laboratory in Grenoble, France. He is currently a Senior Researcher (Automatic Control and Robotics) at the LIRMM laboratory in Montpellier, France. His main research interests include advanced nonlinear control with applications in robotics.

Vincent CREUZE obtained his Ph.D. from the University of Montpellier 2, France, in 2002. Currently, he is a Professor (Accredited to Supervise Research) attached to the Laboratory of Computer Science, Robotics, and Microelectronics (LIRMM), University of Montpellier. His research activities focus more on design, sensing, development, modeling, and robust control applied to underwater vehicles/robots for deep archaeological applications or marine biology.